ACES Asian Chemical Editorial Society

doi.org/10.1002/asia.202300699

CHEMISTRY AN ASIAN JOURNAL Research Article

www.chemasianj.org

Transmission Porosimetry Study on High-quality Zr-fum-MOF Thin Films

Nils Christian Keppler,[a, b] Adrian Hannebauer,[a] Karen Deli Josephine Hindricks,[a, b] Saskia Zailskas,[a] Andreas Schaate,*[a, b] and Peter Behrens+[a, b]

Crystalline Zr-fum-MOF (MOF-801) thin films of high quality are prepared on glass and silicon substrates by direct growth under solvothermal conditions. The synthesis is described in detail and the influence of different synthesis parameters such as temperature, precursor concentration, and the substrate type on the quality of the coatings is illustrated. Zr-fum-MOF thin films are characterized in terms of crystallinity, porosity, and homogeneity. Dense films of optical quality are obtained. The sorption behavior of the thin films is studied with various adsorptives. It can be easily monitored by measuring the transmission of the films in gas flows of different compositions. This simple transmission measurement at only one wavelength allows a very fast evaluation of the adsorption properties of thin films as compared to traditional sorption methods. The sorption behavior of the thin films is compared with the sorption properties of Zr-fum-MOF powder samples.

Introduction

Metal-organic frameworks (MOFs) are an interesting class of porous materials presenting highly adaptable and tunable properties due to their modular composition.[1] As a hybrid material, the framework of these coordination polymers consists of inorganic building units (IBUs) containing metal ions and oxygen atoms; these IBUs are connected by organic linker molecules containing at least two coordinating groups. Both building blocks are highly variable: Many different metals can form IBUs, and depending on the connectivity of the IBU, different structures can be obtained with the same linker molecule.[2,3] The variety of the organic linker molecules is even larger, as linkers can have two or more coordinating sites, such as carboxylates or amines, and a plethora of different functional side groups.[2,4] High inner surface areas and tunable pore sizes are possible.[5] Metal-organic frameworks can be used in many classical applications of porous solids, like catalysis,[6] sensing,[7] gas storage,[8] and gas separation,[9] often with favorable properties. More recently, novel application fields such as optics, electronics, and optoelectronics have come into focus.[10]

However, MOFs often also have drawbacks, such as the low thermal and chemical stability of many frameworks. One example is the low water stability of many MOFs.[11] A solution to this stability issue is the use of zirconium as the metal component. Due to the strong binding between the highly charged Zr^{4+} ions and the coordinating carboxylate groups as well as the high coordination numbers of the IBUs,[12] many zirconium-based MOFs are highly stable. This class of MOFs was introduced by Lillerud and co-workers.[2] Many zirconium MOFs have been well studied, but most of the research has been done on UiO-66 and its derivatives.[13]

Another challenge is the shaping of MOFs. Whereas MOFs are routinely synthesized as powders, and sometimes are generated as single crystals, these are often not the preferred forms for applications. Many applications will benefit from thin films of MOFs,[14,15] e.g. in sensing,[16,17] catalysis,[15,18] and electronic applications.[15,19] Different preparation methods have been reported for the production of MOF thin films, ranging from coatings obtained from particle suspensions by classical coating techniques (such as dip-coating, spin-coating, self-assembly, and drop-casting),[20,21] layer-by-layer growth from precursor solutions (also called liquid phase epitaxy, LPE),[21,22,23] solvent-assisted conversion,[19,24,25] CVD,[26] and direct growth.[27–29] Most of these techniques offer good control over the thickness of the films. The quality of the coatings – as judged by their physical and chemical homogeneity, density, or the absence of voids and cracks – can vary widely, in part because different desired applications impose different quality requirements. These are less stringent, e.g., for catalytic applications, but very strict for membrane applications or in optics. Direct growth methods can produce high-quality films if the synthesis parameters are optimized. For example, high-quality films of ZIF-8,[27] and indium-based MIL-96[30] have been synthesized in this way.

[a] N. C. Keppler, A. Hannebauer, K. D. J. Hindricks, S. Zailskas, Dr. A. Schaate, Dr. P. Behrens+
Leibniz University Hannover
Institute of Inorganic Chemistry
Callinstr. 9, 30167 Hannover (Germany)
E-mail: andreas.schaate@acb.uni-hannover.de

[b] N. C. Keppler, K. D. J. Hindricks, Dr. A. Schaate, Dr. P. Behrens+
Leibniz University Hannover
Cluster of Excellence PhoenixD (Photonics, Optics and Engineering – Innovation Across Disciplines)
Welfengarten 1, 30167 Hannover (Germany)

[+] deceased on 13.01.2023

Supporting information for this article is available on the WWW under https://doi.org/10.1002/asia.202300699

The most popular model system for MOF thin film investigations is HKUST-1,[22,31] but also ZIF-8 and UiO-66 are often preferred systems for such studies.[21,25,27,32] Especially for the Zr-based MOF UiO-66, huge differences can be seen in the quality of the thin films, which is typically evaluated in a first step by SEM images. Coatings prepared from particle suspensions usually result in the formation of inhomogeneous films with large voids between the particle aggregates.[21,29] Better quality is often achieved when vapor-assisted conversion is used.[24,25] Solvothermal direct growth offers the potential to achieve improvements through detailed investigations of the composition of the synthesis solution. Miyamoto and co-workers have shown that the addition of modulators or water can improve the quality of the coatings.[28] The drying process of the thin films can also greatly influence their quality. Zhang *et al.* reported a supercritical drying process that can be used to avoid the formation of cracks during drying of the thin films after the synthesis.[33] Most of the direct coating techniques mentioned above have in common that the synthesis must be performed at elevated temperatures.

In this research, we focus on another Zr-based MOF, the zirconium fumarate MOF (Zr-fum-MOF), which was discovered by our research group.[34] The structure of this framework was derived from powder diffraction data in 2012 and was later confirmed by single crystal X-ray diffraction by Furukawa and co-workers. For no obvious reason, these authors gave the Zr-fum-MOF a second name (MOF-801).[35] The Zr-fum-MOF has a similar structure to UiO-66. Both MOFs share the same IBU but have different linker molecules with two carboxylate groups each: Instead of terephthalate, fumarate anions are present in Zr-fum-MOF. Compared to terephthalate, fumarate is shorted and less rigid – the carbon atoms of the backbone and the carboxylate groups do not lie in a straight line.[34] As a result, the IBUs in the Zr-fum-MOF are slightly tilted with respect to the cubic unit cell axes. The Zr-fum framework is denser than that of UiO-66 and has a lower inner surface area,[34] yet Zr-fum-MOF is still a highly porous material, albeit with smaller pore openings, resulting in preferential sorption of small molecules. For example, Zr-fum-MOF has a high selectivity towards adsorption of water[35–37] and carbon dioxide molecules.[38]

The synthesis has been studied intensively: Zr-fum-MOF can be synthesized in DMF or water and can be obtained as powder and single crystals. Typically, the addition of a modulator is necessary to achieve crystallization and additional water can support the crystallization of the Zr-fum-MOF.[34,35,38,39] Modulators are small molecules such as monocarboxylic acids that allow to control the MOF formation reaction.[16,40] Thin films of the Zr-fum-MOF grown directly on substrates were recently published for the first time by Shekhah and co-workers[41] illustrating how current this topic is. They used an electrochemical approach to synthesize the Zr-fum-MOF thin films on aluminum oxide supports for gas separation applications. The only other achievements in the field of Zr-fum-MOF coatings are about Zr-fum-MOF crystals coated on substrates by loading the crystals in a polymer matrix[42,43] and surface-supported photonic crystals of Zr-fum-MOF and TiO_2 nanoparticles.[44]

With its small pore apertures generated by the small linker, the Zr-fum-MOF has proven to be a practical material for the separation of small molecules such as CO_2/N_2,[45] or light alkanes.[46] Even alkane/alkene separations like propane/propene are possible with fine-tuned defect management.[47] The high affinity and stability towards water makes the Zr-fum-MOF an interesting material, especially for water adsorption-based applications,[48] for example in the field of water harvesting from air and in adsorption cooling.[36,49,50] The combination of the facts that pore filling occurs even at low relative humidity and that desorption occurs at mild temperatures makes the Zr-fum-MOF an excellent material for these applications.[36,50] Furthermore, Chen and co-workers investigated the Zr-fum-MOF for relative humidity sensing by spin-coating nanoparticles onto a TiO_2 substrate.[44] The measured reflectance spectra showed high sensitivity and a good linear fit with increasing relative humidity.

Results and Discussion

In this section, the preparation of Zr-fum-MOF thin films on different substrates in a solvothermal process is described. The synthesis conditions are optimized and the quality of the coatings is verified by XRD, SEM and AFM measurements. In the second part, we focus on the optical characterization of the prepared high-quality thin films using ellipsometry and UV/vis spectroscopy. The changes of the refractive index and the transmission of the Zr-fum-MOF thin films in different gas and vapor atmospheres are investigated, also as a function of the concentration.

Preparation and characterization of Zr-fum-MOF films

The preparation of substrate-supported Zr-fum-MOF thin films of high optical quality has not been described so far. The aim of this study is to prepare these optical coatings. They should be crystalline and highly transparent for this purpose. The crystallinity is important to transfer the chemical properties, especially the porosity, of the MOF to the thin film; the optical quality is important to make these chemical properties accessible for optical measurements. Therefore, the possible synthesis conditions had to be first narrowed down and then optimized. In fact, it is not even known beforehand whether it is possible to form high-quality MOF films from a given synthesis system. In our experiments, we first used glass substrates and then successfully transferred the synthesis conditions to silicon wafers. All syntheses were performed with the substrate side that was later investigated upside down to avoid sedimentation on the investigated sample side.

Zr-fum-MOF can be synthesized solvothermally in the form of particles (as a powder).[34] We have taken as a starting point the synthesis conditions that are used for the synthesis of Zr-fum-MOF powder samples, keeping some of the basic parameters but changing others. We kept the reaction time at 24 hours and the equivalent (eq) ratio of $ZrCl_4$ to fumaric acid at 1:3 for

all syntheses, both like it has been reported before for powder synthesis. In the original synthesis, Zr-fum-MOF is typically crystallized from a solution in DMF (500 eq) containing formic acid as a modulator. When we performed such modulated syntheses in the presence of a substrate, crystalline films were obtained, but the films scattered light strongly and had a white appearance, i.e., were of low quality. Increasing or decreasing the concentration of formic acid did not improve the optical quality of the films. Therefore, we did not use formic acid or any other modulators anymore in this study. On the other hand, previous investigations have shown that minimal amounts of water can strongly influence the formation of Zr-fum-MOF, and that such amounts of water can be supplied by the residual water content always present in the modulator formic acid.[39] When we performed syntheses without modulator (and thus without any water), no crystallization on the substrate surface was observed. This changed when 1 eq of water was added to the synthesis mixture. Therefore, in all the following syntheses, one equivalent of water was added to support crystallization.

The synthesis parameters we have focused on are the reaction temperature and the precursor concentration, which is typically given in terms of DMF equivalents compared to one equivalent of $ZrCl_4$. To gain insight into the thin film formation, the synthesis was carried out at 100, 110 and 120 °C with amounts of 500, 800 and 1000 eq of DMF, respectively – the precursor concentration decreases with increasing eq of DMF. XRD patterns of the resulting coated substrates are shown in Figure 1 for the samples obtained using glass as a substrate (a–c). Crystalline films can be obtained at all temperatures. However, there is a strong influence of temperature: The Zr-fum-MOF crystallizes at all precursor concentrations when a lower reaction temperature of 100 °C is used. This is no longer the case when the temperature is increased. Especially at 120 °C, the reaction window for a crystalline film shifts to lower precursor concentrations (higher DMF amount of 1000 eq). No crystalline films were obtained with higher precursor concentrations (500 or 800 eq of DMF) when the synthesis was performed at 120 °C. Syntheses at 110 °C yield crystalline films when precursor concentrations corresponding to 800 and 1000 eq of DMF are used. Assuming that nucleation on the substrate is strongly favored, this can be explained by differences in the nucleation rates: The nucleation rate increases with temperature and precursor concentration. This is due to the nucleation being an activated process and the supersaturation being higher at higher precursor concentrations. At excessively high nucleation rates, materials may be deposited as amor-

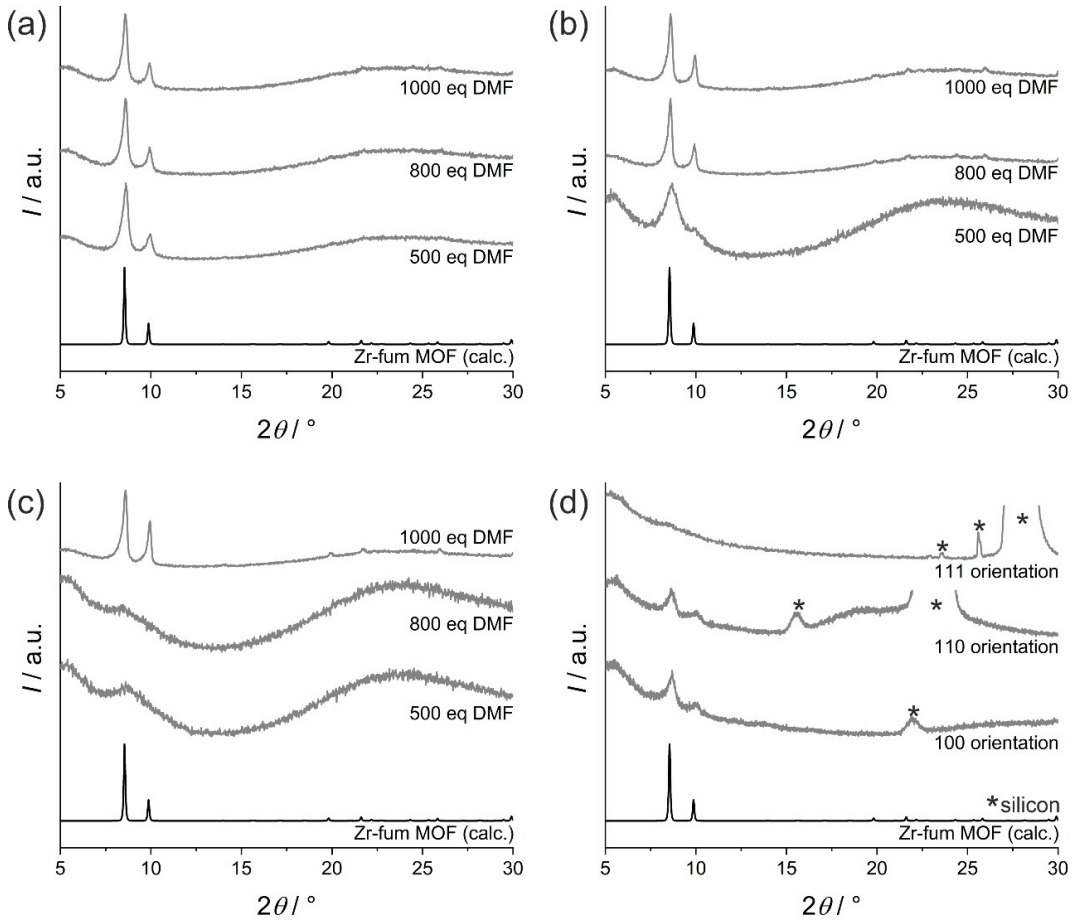

Figure 1. XRD patterns of Zr-fum-MOF thin films synthesized at 100 °C on glass (a), 110 °C on glass (b), 120 °C on glass (c) at different precursor concentrations (given as equivalents of the solvent DMF), and (d) 120 °C on silicon wafers with different orientations of the silicon wafer and at a low precursor concentration, indicated by the use of 1000 eq of DMF solvent. Additional reflections in (d) are attributed to the silicon substrates and are marked with stars (*).

phous solids, as the time for the formation of crystalline nuclei is too short. This is evidently the case here at higher temperatures and higher precursor concentrations (lower amounts of the solvent DMF).

Crystalline films were successfully synthesized at different concentrations and temperatures. This study aims to produce Zr-fum-MOF thin films of optical quality, and thus, the required characteristics of the films are not limited to crystallinity. The thin films must exhibit high optical quality with emphasis on transparency. The required quality is achieved when films have a smooth surface and a minimal occurrence of inhomogeneities, such as crystals growing on or out of the surface or cracks. Ideally, no inhomogeneities or cracks should be present. The surface quality of our thin films was evaluated using SEM. Figure 2 displays typical images of the Zr-fum-MOF thin films on glass that were synthesized at different reaction temperatures and precursor concentrations. These images demonstrate a strong influence of the precursor concentration: The coatings quality is inferior when high precursor concentrations (500 eq of DMF) are used (Figure 2a, d, g). The films exhibit numerous cracks and inhomogeneities covering the entire surface of the films. Despite the presence of cracks, no voids or holes are observed, and the substrate surface is covered with a continuous film. The quality of the thin film is greatly improved by diluting the synthesis: At a reaction temperature of 110 or 120 °C, narrow cracks form only at lower precursor concentrations, specifically at 800 eq of DMF (Figure 2e, h), and disappear completely at the lowest investigated concentration, which corresponds to 1000 eq of DMF (Figure 2f, i). In addition to the cracks, all samples show inhomogeneities in the form of dots on the surface. These could be particles that formed through secondary nucleation, which means they initially nucleated on the formed thin film and not on the substrate. At higher dilution of the synthesis solution or at higher temperatures, when the supersaturation is lower, these inhomogeneities become smaller and less numerous. This indicates that the dilution of the precursor solution improves the quality of the Zr-fum-MOF thin films. At 120 °C and highly diluted synthesis solutions (1000 eq of DMF), only a few small inhomogeneities appear on the Zr-fum-MOF thin films (Figure 2i).

According to XRD and SEM studies, the Zr-fum-MOF thin films exhibit superior quality at higher reaction temperatures and higher dilutions of the synthesis solution. Therefore, a reaction temperature of 120 °C and a precursor concentration corresponding to 1000 eq of DMF solvent were chosen as the standard conditions. The films prepared using these parameters were thoroughly characterized. In some optical characterizations, like refractive index measurements, it is necessary to present the thin films on reflecting surfaces such as silicon substrates. The growth of the MOF was tested on silicon wafers with different orientations, including 100, 110 and 111. Figure 1d displays the XRD patterns of the resulting coatings. On silicon wafers with 100 and 110 orientation, crystalline thin films of Zr-fum-MOF were obtained. The reflections match well with those of a calculated XRD of the Zr-fum-MOF. No reflections of the MOF structure were visible in the XRD of the attempted

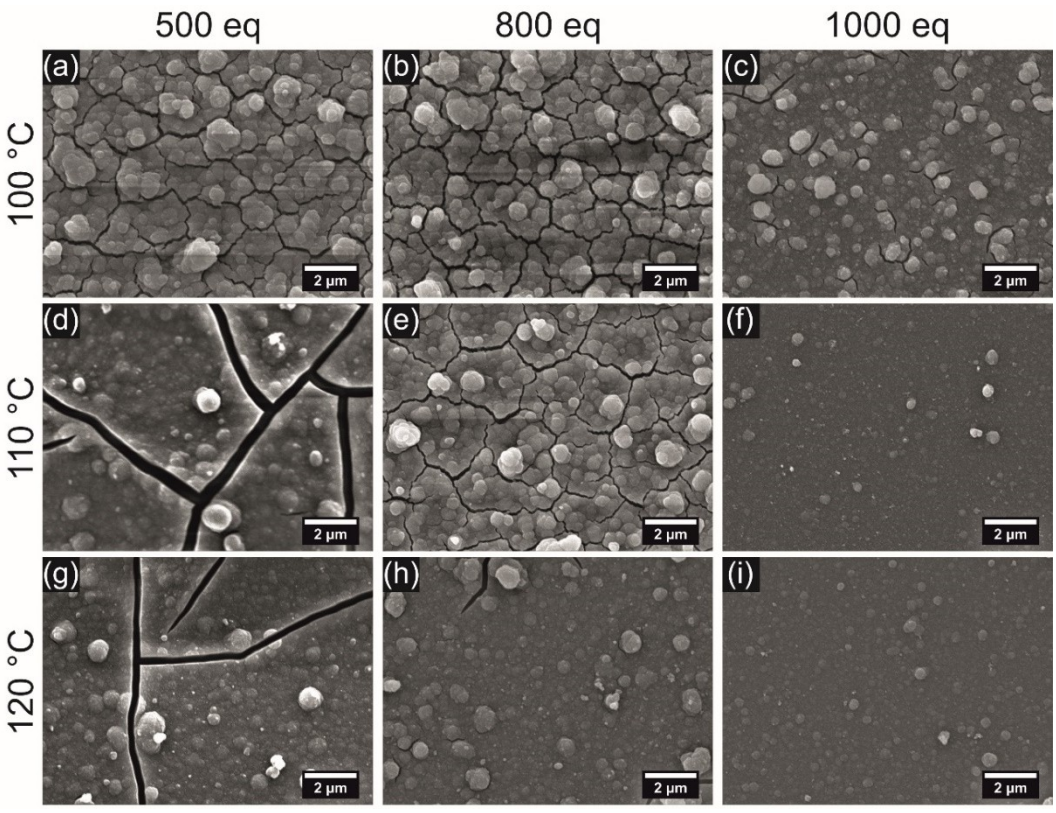

Figure 2. SEM images of Zr-fum-MOF thin films on glass substrates, synthesized using different reaction temperatures and precursor concentrations (in equivalents of DMF).

coating on a silicon wafer with 111 orientation; instead of forming the MOF, an amorphous film was formed. The reflections present are solely caused by the silicon substrate. We opted to utilize silicon wafers with 100 orientation for the further characterizations. SEM images of such a Zr-fum-MOF thin film are provided in Figure 3. Image (a) shows a top view of the coated surface. The film's surface shows no cracks and only a few inhomogeneities are visible. Figure 3 b displays the cross-sectional image, which illustrates that a dense and homogeneous film with a thickness of around 150 nm has formed on the substrate surface. A cross-sectional SEM image of a thin film fabricated on glass is presented in Figure S1 (Supporting Information). The thin film has a thickness of approximately 200 nm, indicating that its growth varies slightly on different substrates. However, a dense, homogeneous, and thin coating is still formed on the substrate.

Surface roughness of the Zr-fum-MOF thin films was analyzed using atomic force microscopy (AFM). A representative AFM image is shown in Figure 4. The AFM image correlates with the SEM images of analogously prepared samples shown in Figure 2i and Figure 3a. All the images only exhibit small inhomogeneities. From five measurement spots, a surface roughness of $R_a = (9.6 \pm 1.1)$ nm was measured. Further AFM data can be found in Figure S2 (Supporting Information).

Krypton physisorption measurements were performed to analyze the porosity of the thin films. Krypton was chosen due to the low amount of coating present in thin films. The isotherm is illustrated in Figure 5. Its course resembles the type I isotherms typical for microporous materials[51] and that the argon physisorption measurements of crystalline Zr-fum-MOF powder samples (see Figure S3, Supporting Information). According to the BET analysis of the given isotherm, the thin films have a surface area of 320 cm^2/cm^2.

Optical characterization of Zr-fum-MOF thin films

This chapter aims to evaluate the optical properties of the Zr-fum-MOF thin films. To gain insights into the properties of the thin films and to their capabilities for applications in the sorption of gases, ellipsometry and UV/vis spectroscopy were used. The resulting data are carefully compared with those obtained by sorption measurements on Zr-fum-MOF powder samples.

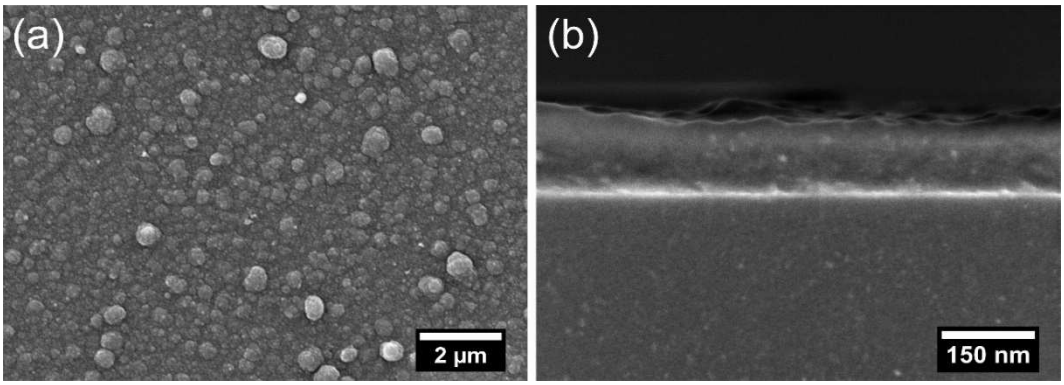

Figure 3. SEM top-view (left) and cross-sectional (right) images of a Zr-fum-MOF thin film on a silicon wafer with 100 orientation (synthesis conditions: 120 °C and 1000 eq of DMF).

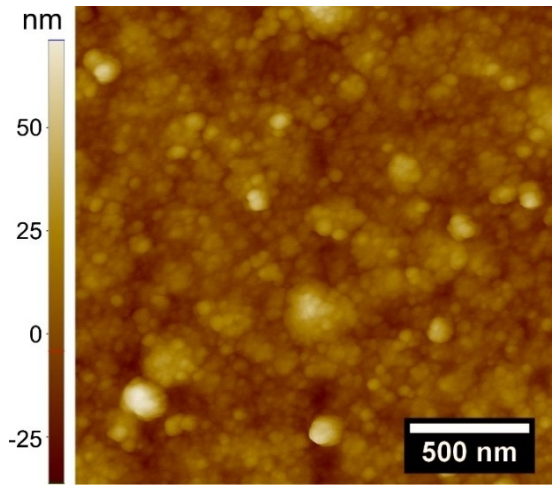

Figure 4. AFM topology image of a Zr-fum-MOF thin film on a silicon substrate with 100 orientation, produced with the optimized synthesis conditions (120 °C and 1000 eq of DMF).

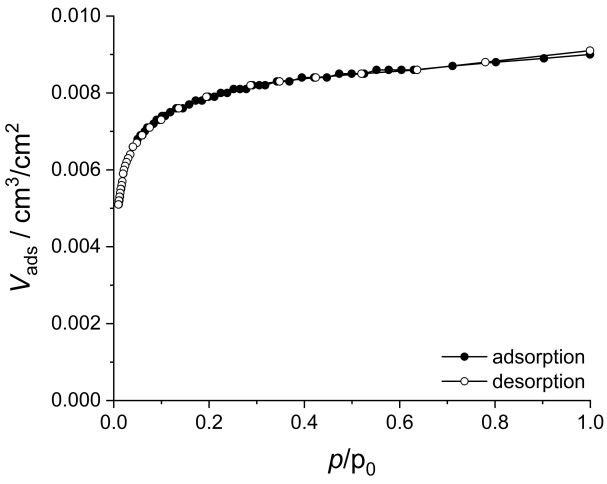

Figure 5. Krypton physisorption isotherm of Zr-fum-MOF thin films on silicon substrates with 100 orientation, produced with the optimized synthesis conditions (120 °C and 1000 eq of DMF). The isotherm was measured at 87 K.

Figure 6 shows a UV/vis transmission spectrum and a photograph of Zr-fum-MOF coated glass slides. Uncoated glass is provided as a reference material. The Zr-fum-MOF-coated glass slide is almost as transparent as the uncoated glass. Figure 7 displays the results obtained through ellipsometry measurements. The decay of the refractive index predominates over the visible spectrum, as shown by the results of the Tauc-Lorentz model with two oscillators displayed in Figure 7a. This is in good agreement with the UV/vis spectrum of the Zr-fum-MOF-coated glass and the powder sample (see Figure S5 a, Supporting Information), displaying no absorption bands in the visible light range. Absorption of light would cause anomalous dispersion – resulting in a turning point in the refractive index around the absorption maximum. No absorption from the band gap of the Zr-fum-MOF is expected. The MOF powder exhibits absorption in the UV range of the light spectrum. The band gap was determined to be 4.6 eV using a Tauc plot (refer to Figure S5 b, Supporting Information). A decrease of the refractive index over the visible light range is observed at increasing wavelengths, as is typical for colorless materials.

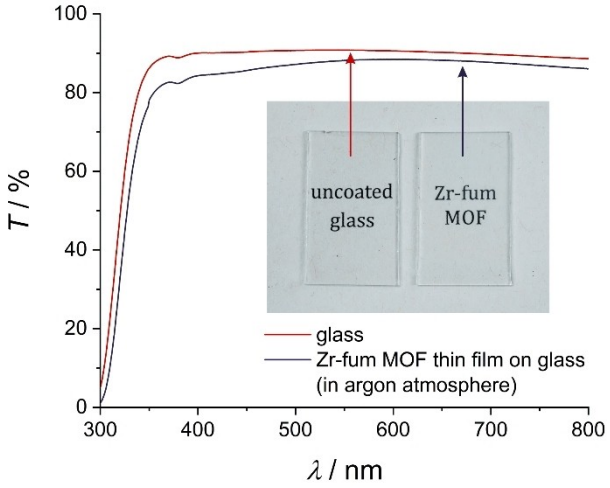

Figure 6. UV/vis transmission spectra and photography of uncoated (red) and Zr-fum-MOF-coated (blue) glass slides. The text is printed on a paper placed behind the glass slides.

Figure 7b shows a plot of the experimental and fitted data for the amplitude ratio Ψ and the phase difference $\triangle$ for a typical ellipsometry measurement on a Zr-fum-MOF thin film. The model and experimental data exhibit a good agreement, supported by a low mean squared error (MSE) of 2.6 of the ellipsometry fit. From the ellipsometry fit, the refractive index is calculated to be 1.646 at 589 nm. Compared to the bulk ZrO_2, this value is significantly lower (2.1 at 550 nm)[52] due to the porosity of the MOF. However, it is higher than that of other MOFs like ZIF-8 or HKUST-1,[22,53] which can be attributed to the presence of Zirconium that provides much more electrons than zinc or copper and by the comparably high density of the Zr-fum-MOF. Both factors (electron density and density) contribute to the increase of the refractive index. According to the ellipsometry fit, the thickness of the thin film is 188 nm which is consistent with the cross-sectional SEM measurement (see Figure 3b).

Measurements of the refractive index in various atmospheres, such as argon, methane, carbon dioxide, and argon that is saturated with ethanol or water, lead to different values. All measurements show an increase of the refractive index when compared to measurements carried out in argon atmosphere. According to the pore-filling model that was introduced in the MOF community by the Hupp group,[27] an increase of the refractive index of a MOF can be correlated to the adsorption of a guest. This suggests that all the analytes investigated can be adsorbed in the Zr-fum-MOF thin films. Large refractive index changes of up to 0.06 were obtained especially in water and ethanol-containing atmospheres at lower wavelengths. To obtain a deeper understanding of the sorption process of these guests, sorption studies were performed on Zr-fum-MOF powder samples using classical static gas or vapor physisorption measurements and on the Zr-fum-MOF thin films non-classical dynamic transmission porosimetry measurements.

Next, we will compare the adsorption properties of the high-quality Zr-fum-MOF thin films with those of the corresponding bulk samples (powders). As previously stated in the introduction and evidenced by the increase of the refractive index in a moist atmosphere compared to dry argon (refer to

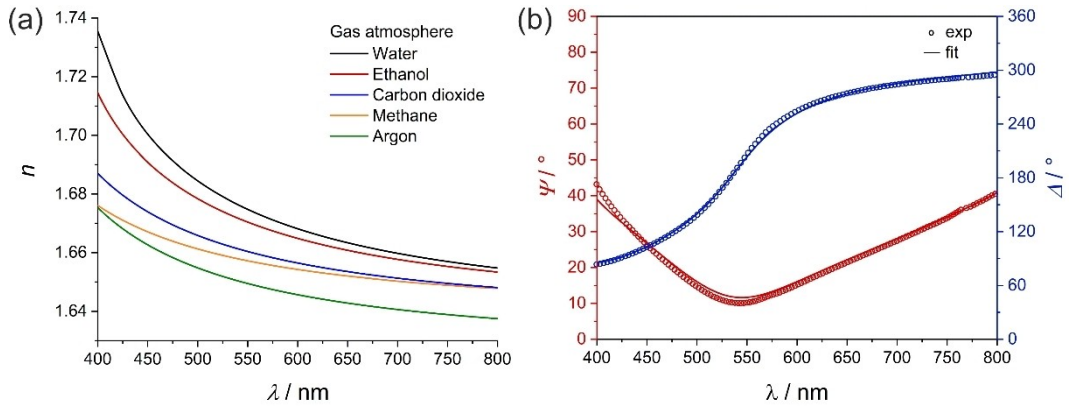

Figure 7. Ellipsometry investigation of Zr-fum-MOF thin films. The refractive index dispersions in different gas atmospheres (a) and a plot of the experimental (circles) and fitted (line) ellipsometry data, the amplitude ratio Ψ and the phase difference $\triangle$, (b) are shown. The measurement in (b) was performed in argon atmosphere. Thin films on silicon (100 orientation), prepared using optimized synthesis conditions (120 °C and 1000 eq of DMF), were used.

Figure 7a), it is known that the Zr-fum-MOF efficiently adsorbs water.[35–37] We reproduced the sorption isotherms for water, carbon dioxide and methane on powder samples and added data for ethanol (refer to Figure 8a). Both isotherms show a high affinity for water and ethanol, particularly at low pressures below 1 kPa. Water adsorption occurs at a low relative pressure below 0.2, which is consistent with water sorption data published by other research groups.[35,37,42,48,54] Nevertheless, some deviations between the published water sorption isotherms are present. These deviations could be caused for example by the particle size or morphology. The Yaghi group received slightly different water sorption isotherms for Zr-fum-MOF (micrometer-sized) powders and single crystals,[35] while Han and co-workers reported an even more pronounced shift of the isotherm towards lower relative water pressure.[54] However, due to the lack of SEM images or related information about the crystal size or morphology, no definitive statement can be made regarding the influence of MOF particle shape. Additionally, it should be noted that the thin film shape may also slightly shift the position of the main uptake of water and other adsorptives. Adsorption of carbon dioxide and methane also occurs, albeit at lower levels. This is due, at least in part, to their higher saturation pressures relative to water and ethanol. There is once again a good agreement with published data, confirming a higher uptake for CO_2 compared to methane.[38,42,43,46]

Characterizing the pore system of thin films is more challenging than that of powders. This is because of the small amount of material present in films with thicknesses of a few hundred nanometers and the possibility of substrate interferences. Thus, special methods and instruments are used to characterize thin films.[55] These include widely used methods such as quartz crystal microbalance (QCM), physisorption carried out manometrically/volumetrically with krypton gas (like krypton physisorption, as used in this work, see Figure 5) and ellipsometric porosimetry (EP). While positron annihilation lifetime spectroscopy (PALS) can provide detailed information, it requires more elaborate equipment.[55] Ellipsometry measurements determine changes in light polarization upon specular reflection and are typically done at multiple wavelengths in the visible range. The refractive index of the thin film changes when a guest species is adsorbed at different partial pressures. The refractive index can be calculated for each partial pressure using an appropriate model and a fit procedure (see Figure 7b and Table S1). It should be noted that the calculated refractive index values are a result of the fit procedure and are not directly measured. From this point on, we would like to shift the focus from ellipsometry-based porosimetry to transmission-based porosimetry. In the following ellipsometry will be used only for further validation of the results.

Here, we propose a new optical method to characterize the sorption behavior of thin films in a shorter time than traditional methods, such as sorption on powder samples with gas or vapor, without making further assumptions. To use this method, thin films of optical quality are required. The method entails measuring the transmission of the sample at a fixed wavelength of the visible light spectrum at increasing partial pressure of the adsorptive in an inert gas flow. The method can be easily executed with a home-built measurement cell that has quartz glass windows and a gas inlet and outlet to allow transmission measurements of thin films in a controllable gas atmosphere and thus to study the sorption properties of the thin films due to transmission changes caused by guest adsorption in the MOF pores. Mass-flow controllers are utilized for regulating the composition of two distinct gas flows: One of the flows contains the guest, while the other serves the purpose of purging or diluting the guest gas flow with an inert gas, such as argon. There are two methods to introduce an analyte into the guest flow: (i) gas method: When the guest is a gas such as carbon dioxide or methane, its gas stream is mixed with argon directly before it reaches the measurement cell; (ii) vapor method: A reservoir filled with a liquid such as water or ethanol is inserted in one of the two argon gas flows before the two flows are mixed. The liquid evaporates as argon gas passes through it. In the vapor method, the guest content of the argon flow with the liquid inserted is set to 100%; it should correspond to the saturation vapor pressure of the substance in argon. Dilution of guest content to the desired value can be achieved by

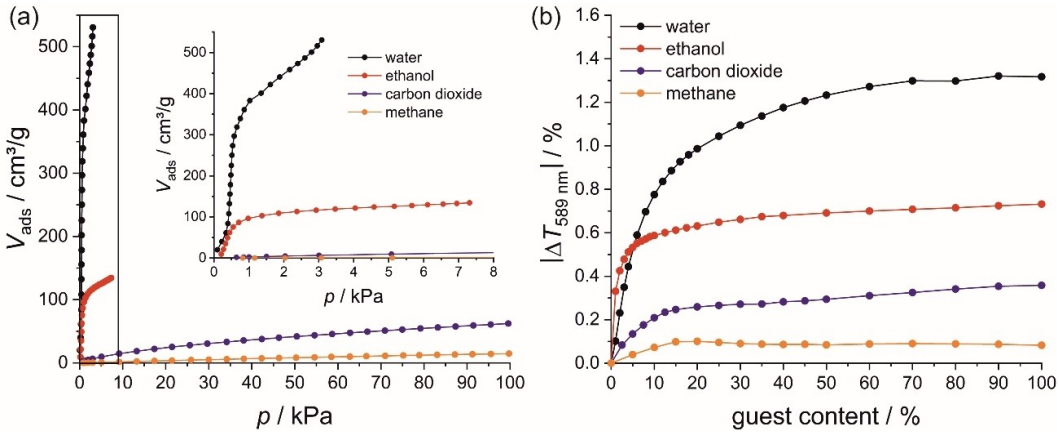

Figure 8. Adsorption isotherms of Zr-fum-MOF, measured on powders (a) and on thin films (b). Isotherms are shown for the adsorptives methane, carbon dioxide, ethanol and water. Measurements on powders were made volumetrically, while measurements on thin films were performed using transmission measurements at 589 nm for different guest contents in a gas flow.

introducing argon from the second gas flow. Further details are provided in the Supporting Information: Schemes of both setups are shown in Figure S6; a detailed description of how the data is analyzed can be found in Figure S7 and the accompanying text.

The results of the transmission porosimetry measurements are shown in Figure 8b. The figure displays the absolute transmission change for various adsorptive contents in the gas flow, ranging from 0 to 100% for all guests, in comparison to the transmission at a guest content of 0% at a wavelength of 589 nm. It is advisable to be cautious when comparing these adsorption curves with those measured on the Zr-fum-MOF powder samples. The latter are obtained through standard vapor sorption measurements, where the adsorptive gas is the only gas present. The volume uptakes are subsequently correlated with the gas pressure. In contrast, transmission sorption measurements reflect the adsorption of a gas component from a dynamic flow of a gas mixture. It is not possible to establish a direct correlation between the pressure scales used in volumetric measurement and partial pressure in a gas mixture in the transmission porosimetry measurement.

A semi-quantitative comparison between the two measurements (both depicted in Figure 8) is possible and reveals additional insights. The sequence of the adsorptives regarding sorption capacity is identical for powder and film measurements. Additionally, the general shape of the sorption isotherms appears similar. Nonetheless, some differences could be linked to the sample morphology. In the powder sample, the particles contribute a substantial outer surface area and also interparticular voids are present. The high-quality thin films prepared within this work are dense, resulting in negligible outer surface area and a negligible amount of interparticular voids. In this context, the sorption isotherms of water and ethanol are particular interesting. In the standard vapor phase sorption experiment, ethanol exhibits a type I like isotherm. Saturation is reached at about $p \approx 1$ kPa with an adsorbed volume of ≈ 100 cm^3/g. The powder sample also attracts water easily, yielding an uptake of ≈ 400 cm^3/g at $p \approx 1$ kPa. The uptake of water increases continuously at higher pressures. In the transmission experiment, ethanol behaves similarly to the vapor phase sorption, with saturation nearly attained at approximately 10% ethanol content in the gas phase that is offered for adsorption. However, water reaches saturation only at around 50% concentration in the gas phase. The rapid increase in the sorption curves in the transmission porosimetry measurements due to a small amount of adsorptive in the gas phase is consistent with the standard vapor sorption experiment: Ethanol is adsorbed at a lower gas phase content, indicating a stronger affinity of the inner pore system of Zr-fum-MOF for ethanol compared to water. The same scenario holds for the standard vapor sorption experiment on the powder sample when the guest content is presented as relative pressure (see Figure 9). At a relative pressure below 0.1, a larger quantity of ethanol compared to water is adsorbed. The observed differences in water sorption could potentially be elucidated by the following model: The powder sample displays adsorption sites on the outer surface of the particles which

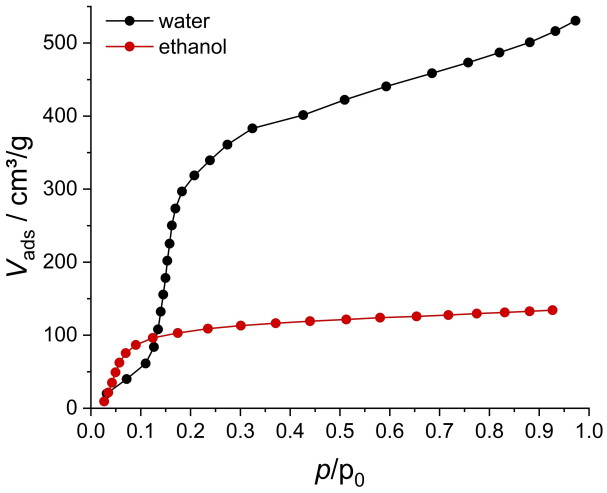

Figure 9. Standard vapor sorption isotherms of Zr-fum-MOF powder samples using ethanol and water as adsorptives, given in relative pressure. The isotherms were measured at 25 °C

have a strong affinity for water, potentially due to the presence of under-coordinated metal ions of the IBUs resulting from missing linkers on the surface.[56] Adsorption initiates at these sites and then proceeds in tandem with regular adsorption in the pore system, ultimately leading to a high uptake of approximately 400 cm^3/g at $p \approx 1$ kPa. Above that pressure, additional water is taken up, likely condensing in the interparticle voids. No distinctive effects are observed in the transmission measurements on thin films: There are few active sites on the outer surface and no voids between the individual crystals. The inner pore system is regularly filled with water and ethanol, with ethanol having a higher affinity to the pore system at low guest contents.

Both methane and carbon dioxide, investigated using the gas method, showed low uptakes as was measured on the powder samples. Carbon dioxide adsorption is clearly preferred over methane adsorption. The same result is also obtained in the transmission porosimetry measurements: A low transmission change is visible in the presence of methane due to its low amount adsorbed, especially when compared to the changes that are obtained by water and ethanol adsorption. The adsorption of carbon dioxide causes an approximately three-fold increase in transmission change, indicating a higher affinity of the Zr-fum-MOF towards CO_2. A similar result is obtained from the refractive index measurements on Zr-fum-MOF thin films in argon, methane and carbon dioxide atmosphere (see Figure 7a): Although CO_2 and methane lead to only a small increase of the refractive index of the thin films, CO_2 induces a higher refractive index change due to its higher affinity towards the Zr-fum-MOF pore system. Overall, the results from standard gas/vapor sorption, transmission porosimetry and ellipsometry measurements show good qualitative agreement in the atmospheres of all guest molecules: The guest molecules affinity to the MOF is found to be in the same order, with water having the highest impact on the refractive index of the Zr-fum-MOF ($\Delta n_D = 0.023$), followed by ethanol (0.020),

carbon dioxide (0.011) and finally methane, which induces the lowest refractive index change (0.008).

The results of the sorption studies indicate that the newly proposed transmission porosimetry method could widen the accessible range of porosimetric measurements for the characterization of (MOF) thin films using a fast and easy-to-implement measurement approach.

Conclusions

The Zr-fum-MOF (MOF-801) is an interesting representative of metal-organic frameworks that has been reported in different shapes, except for thin films of optical quality. We have demonstrated that the Zr-fum-MOF can be prepared as a thin film using a direct solvothermal growth method. In this procedure glass and silicon substrates can be used as supports in this procedure. Of the large number of different MOFs known (more than 100,000),[57] only a few have been prepared as thin films, and even fewer as thin films with optical quality. Direct growth on the substrate has proven to be an effective method for generating high-quality films.[27,30] However, there is no universal recipe for synthesizing thin films and the conditions need to be optimized for each specific system.

We successfully optimized these synthesis conditions yielding dense, homogeneous, and crack-free films with high (optical) quality. Thorough characterization of the films was conducted. The porosity of the films was validated by krypton porosimetry. The optical properties of the thin films were studied using UV/vis spectroscopy and ellipsometry: The band gap of Zr-fum-MOF was determined to be 4.6 eV and its refractive index at 589 nm was measured to be 1.646 under dry argon atmosphere. The possibility of producing high-quality thin films of the Zr-fum-MOF on standard substrates such as glass and silicon makes this highly stable MOF a potential component in optical devices like photonic crystals or waveguides. The refractive index and transmission of the material can be tuned by adsorption of molecules if desired.

We conducted additional characterization on the thin films and compared them to Zr-fum-MOF powder samples regarding the adsorption of various analytes such as water, ethanol, carbon dioxide and methane. The thin films were characterized by transmission measurements at a fixed wavelength using analyte and inert gas mixtures as adsorptives. Overall, the trends for sorption of the various substances seem to be similar for both the Zr-fum-MOF powder and thin films. The discernible differences are mainly found for the sorption of water, which may be due to the different sample morphologies: The standard measurement of the powder could be affected by the large outer surface area of the particles and the interparticle condensation.

The ability to generate thin films of the Zr-fum-MOF can have various applications beyond the current focus, such as using supported membranes to separate of hydrocarbons or accelerating the kinetics of water uptake and release in water harvesting.

Experimental Section

Materials

Silicon wafers (diameter 4 inches) were ordered from Micro-Chemicals (100, 110 and 111 orientation). Glass substrates with cut edges (75×26 mm) were ordered from VWR.

Ethanol (99.8%, Fisher-Scientific), *N*,*N*′-dimethylformamide (99.8%, Sigma-Aldrich, DMF), zirconium(IV) chloride (99.5%, Sigma-Aldrich, $ZrCl_4$), fumaric acid (98%, Sigma-Aldric), formic acid (98%, Merck), acetone (99.5%, Roth), sulfuric acid (96%, Roth), hydrogen peroxide solution in water (35%, Roth), hydrogen chloride solution in water (Roth, 37%) and sodium hydroxide (Honeywell, 98%) were used without further purification. Methane and carbon dioxide gas were ordered from Linde.

Preparation of thin films

Glass slides and silicon wafers were cut into pieces measuring 16×26 mm. All substrates were cleaned in a freshly prepared mixture of sulfuric acid and hydrogen peroxide (2:1) for 15 min. Subsequently, they were rinsed with water and twice with ethanol and dried in air before use.

To minimize solvent and precursor usage, films were prepared by filling a 10 mL vial with 8 mL synthesis solution and leaving it uncovered. Substrates were directly put into the 10 mL vial. Afterwards, the 10 mL vial was transferred into a 100 mL glass flask that was secured with a teflon-cap. The transfer to the 100 mL flask is necessary to ensure that the solvent does not completely evaporate from the synthesis solution, since the 10 mL vials cannot be sealed tightly. A typical synthesis solution always contained 1 equivalent (eq) $ZrCl_4$, 3 eq fumaric acid and 1 eq of water, dissolved in DMF at different concentrations ranging from 500 to 1000 eq of DMF using ultrasonication. The capped vessels were heated in an oven for 24 h at 100 to 120 °C. After heating, the vessels were allowed to cool down to room temperature (ca. 15 minutes). The coated substrates were rinsed with ethanol. It is important to note that the side of the substrate that was used for the investigations and measurements was put upside down in synthesis solution. This prevents sedimentation on the backside of the samples.

The substrates underwent either direct use (XRD and SEM) or overnight storage in ethanol (ellipsometry, krypton physisorption and UV/vis spectroscopy) to remove unreacted precursors and solvent molecules from the pores. The backside of the samples used for sorption experiments (krypton physisorption and transmission measurements) underwent careful cleaning with tissue papers soaked first in 2 M sodium hydroxide solution and the second in 2 M hydrogen chloride solution, then followed by water. Afterwards, the samples were dried thoroughly.

Synthesis of powder samples

For comparison purposes, powder samples of the Zr-fum-MOF were synthesized in 100 mL glass flasks according to the procedure detailed elsewhere:[34] $ZrCl_4$ (1 eq) was dissolved in 20 mL DMF (500 eq). Formic acid (50 eq) and fumaric acid (3 eq) were added and dissolved under ultrasonication. The glass flask was teflon-capped and heated in an oven for 24 h at 120 °C. Following cooling to room temperature, the powder was centrifuged, washed with DMF and twice with ethanol and then dried overnight under reduced pressure. Finally, the dry powder was Soxhlet-extracted with acetone for 24 h and then vacuum-dried overnight before

conducting characterization, which included XRD, sorption and UV/vis spectroscopy.[34]

Characterization of films and powder

XRD measurements on Zr-fum-MOF thin films were carried out with an X-ray diffractometer from Stoe working in Bragg-Brentano geometry. An Iso-Debyeflex 3003 was used for the delivery of X-rays at 40 kV and 30 mA. Monochromation of the X-rays occurs in front of the detector, delivering Cu$K\alpha_1$ radiation. Measurements were carried out between 5 and 30° 2θ with a step size of 0.02° 2θ and a measuring time of 8 s per step.

SEM images were recorded with a JSM-6610L V (Joel). Images were taken at 10 kV with a working distance of 10 mm. Additionally, cross-sectional images were recorded using a JSM-6700-F (Joel). The voltage was set to 2 kV at a working distance of 3 mm.

Krypton physisorption isotherms on thin films were measured at 87 K on an Autosorb 1 instrument from Quantachrome and were evaluated with the software ASiQwin 2.0 (Quantachrome). Prior to the measurements, the samples were degassed under vacuum at 120 °C for 24 h. Surface areas were determined by applying the Brunauer–Emmett–Teller (BET) equation.

Argon physisorption measurements on powders were performed at 87 K on a 3Flex instrument from Micromeritics. The powder samples (25 mg) were activated at 120 °C in vacuum for 20 h. For the analysis of the data the associated software from Micromeritics was used. Surface areas were determined using the BET-auto function of the software and total pore volumes were calculated using the single-point method at a relative pressure of 0.95.

Carbon dioxide and methane sorption were measured on an ASAP 2020 instrument from micromeritics at 25 °C. Before the measurements, the Zr-fum-MOF powder sample (50 mg) was activated at 120 °C in vacuum for 20 h.

Static vapor sorption measurements (water and ethanol) were performed on a Vapor 100 C from 3P instruments. The vapor source, either water or ethanol, was purified three times using a freeze-drying method. The temperature of the vapor source was then kept constant at 40 °C for water and 30 °C for ethanol. The Zr-fum-MOF powder sample (50 mg) was activated at 120 °C in vacuum for 20 h. Additionally, the MOF was activated *in-situ* at 120 °C for 4 hours before each measurement. The measurement was performed at a temperature of 25 °C.

AFM measurements were performed using a NX 10 by Park System Corp. Images were taken in non-contact mode with a scan rate of 0.5 Hz and a picture size of 2 μm x 2 μm. The software "XEI" (5.2.0 by Park System Corp.) was used for the data analysis.

UV/vis spectra were recorded on powders and coated glass slides. A Cary 4000 (Agilent Technologies) was employed for all measurements using the software "Scan". The powder sample was investigated in the wavelength range between 200 and 800 nm. Barium sulfate was used for measurement of the background. A Praying Mantis (Harrick) was used for the measurement. Glass slides were investigated in a home-built measurement cell with quartz glass windows and an inlet and outlet for gases. Full spectra of samples on glass were measured in the wavelength range from 300 to 800 nm. Additionally, measurements at a fixed wavelength of 589 nm in variable gas atmospheres were performed using the software "Kinetics" that is part of the software package of the UV/vis spectrometer. Argon was measured as the background for all samples on glass slides. Further information about the experiment are given below in the "results and discussion" section and in Figure S6. Details about the evaluation of the experiments are provided in Figure S7.

A Sentech SE800 spectroscopic ellipsometer with a spectral range of 400 to 850 nm was used for the ellipsometry measurements. Measurements were performed at 70° in an argon flow. Ellipsometry data were fitted with a Tauc-Lorentz dispersion model with roughness layer. More information on the model used to fit the ellipsometry data is given in Table S1.

Acknowledgements

N. C. K. and A. H. contributed equally to this work. This work was funded by the Deutsche Forschungsgemeinschaft (DFG) under Germany's Excellence Strategy within the Cluster of Excellence PhoenixD (EXC 2122, Project ID 390833453). Adrian Hannebauer thanks the hsn (Hannover School for Nanotechnology) for a scholarship. Karen Hindricks thanks the Studienstiftung des Deutschen Volkes (German National Academic Foundation) for a scholarship. We want to thank Younes Senft for building the UV/vis measurement cell. Additionally, we would like to thank Marvin Treger for help with the Tauc plot. Open Access funding enabled and organized by Projekt DEAL.

Conflict of Interests

The authors declare no conflict of interest.

Data Availability Statement

The data that support the findings of this study are available from the corresponding author upon reasonable request.

Keywords: Metal-organic frameworks · MOF thin films · optical applications · porosimetry · Zr-fum-MOF

[1] H.-C. Zhou, J. R. Long, O. M. Yaghi, *Chem. Rev.* **2012**, *122*, 673–674.
[2] J. H. Cavka, S. Jakobsen, U. Olsbye, N. Guillou, C. Lamberti, S. Bordiga, K. P. Lillerud, *J. Am. Chem. Soc.* **2008**, *130*, 13850–13851.
[3] a) C. Serre, F. Millange, C. Thouvenot, M. Noguès, G. Marsolier, D. Louër, G. Férey, *J. Am. Chem. Soc.* **2002**, *124*, 13519–13526; b) B. Panella, M. Hirscher, *Adv. Mater.* **2005**, *5*, 538–541.
[4] a) K. S. Park, Z. Ni, A. P. Côté, J. Y. Choi, R. Huang, F. J. Uribe-Romo, H. K. Chae, M. O'Keeffe, O. M. Yaghi, *Proc. Natl. Acad. Sci. USA* **2006**, *103*, 10186–10191; b) E. D. Bloch, L. J. Murray, W. L. Queen, S. Chavan, S. N. Maximoff, J. P. Bigi, R. Krishna, V. K. Peterson, F. Grandjean, G. J. Long et al., *J. Am. Chem. Soc.* **2011**, *133*, 14814–14822; c) H. Hahm, K. Yoo, H. Ha, M. Kim, *Inorg. Chem.* **2016**, *55*, 7576–7581.
[5] S. Chavan, J. G. Vitillo, D. Gianolio, O. Zavorotynska, B. Civalleri, S. Jakobsen, M. H. Nilsen, L. Valenzano, C. Lamberti, K. P. Lillerud et al., *Phys. Chem. Chem. Phys.* **2012**, *14*, 1614–1626.
[6] a) A. H. Chughtai, N. Ahmad, H. A. Younus, A. Laypkov, F. Verpoort, *Chem. Soc. Rev.* **2015**, *44*, 6804–6849; b) C. A. Trickett, A. Helal, B. A. Al-Maythalony, Z. H. Yamani, K. E. Cordova, O. M. Yaghi, *Nat. Rev. Mater.* **2017**, *2*, 17045.
[7] a) M. Woellner, S. Hausdorf, N. Klein, P. Mueller, M. W. Smith, S. Kaskel, *Adv. Mater.* **2018**, *30*, 1704679; b) M. D. Allendorf, R. Dong, X. Feng, S. Kaskel, D. Matoga, V. Stavila, *Chem. Rev.* **2020**, *120*, 8581–8640; c) J. E. Ellis, S. E. Crawford, K.-J. Kim, *Mater. Adv.* **2021**, *2*, 6169–6196.

[8] a) D. Gygi, E. D. Bloch, J. A. Mason, M. R. Hudson, M. I. Gonzalez, R. L. Siegelman, T. A. Darwish, W. L. Queen, C. M. Brown, J. R. Long, *Chem. Mater.* **2016**, *28*, 1128–1138; b) Y. Ji, L. Ding, Y. Cheng, H. Zhou, S. Yang, F. Li, Y. Li, *J. Phys. Chem. C* **2017**, *121*, 24104–24113; c) X. Yang, Q. Xu, *Cryst. Growth Des.* **2017**, *17*, 1450–1455.
[9] a) U. Böhme, B. Barth, C. Paula, A. Kuhnt, W. Schwieger, A. Mundstock, J. Caro, M. Hartmann, *Langmuir* **2013**, *29*, 8592–8600; b) L. Fan, Z. Kang, Y. Shen, S. Wang, H. Zhao, H. Sun, X. Hu, H. Sun, R. Wang, D. Sun, *Cryst. Growth Des.* **2018**, *18*, 4365–4371; c) A. Knebel, B. Geppert, K. Volgmann, D. I. Kolokolov, A. G. Stepanov, J. Twiefel, P. Heitjans, D. Volkmer, J. Caro, *Science* **2017**, *358*, 347–351.
[10] a) O. Shekhah, J. Liu, R. A. Fischer, C. Wöll, *Chem. Soc. Rev.* **2011**, *40*, 1081–1106; b) I. Stassen, N. Burtch, A. Talin, P. Falcaro, M. Allendorf, R. Ameloot, *Chem. Soc. Rev.* **2017**, *46*, 3185–3241; c) J. F. Olorunyomi, S. T. Geh, R. A. Caruso, C. M. Doherty, *Mater. Horiz.* **2021**, *8*, 2387–2419; d) Z.-G. Gu, A. Pfriem, S. Hamsch, H. Breitwieser, J. Wohlgemuth, L. Heinke, H. Gliemann, C. Wöll, *Microporous Mesoporous Mater.* **2015**, *211*, 82–87.
[11] a) L. N. McHugh, M. J. McPherson, L. J. McCormick, S. A. Morris, P. S. Wheatley, S. J. Teat, D. McKay, D. M. Dawson, C. E. F. Sansome, S. E. Ashbrook et al., *Nat. Chem.* **2018**, *10*, 1096–1102; b) J. J. Low, A. I. Benin, P. Jakubczak, J. F. Abrahamian, S. A. Faheem, R. R. Willis, *J. Am. Chem. Soc.* **2009**, *131*, 15834–15842.
[12] a) T. Devic, C. Serre, *Chem. Soc. Rev.* **2014**, *43*, 6097–6115; b) W. Liang, H. Chevreau, F. Ragon, P. D. Southon, V. K. Peterson, D. M. D'Alessandro, *CrystEngComm* **2014**, *16*, 6530–6533.
[13] J. Winarta, B. Shan, S. M. Mcintyre, L. Ye, C. Wang, J. Liu, B. Mu, *Cryst. Growth Des.* **2020**, *20*, 1347–1362.
[14] a) Z. Wang, C. Wöll, *Adv. Mater. Technol.* **2019**, *4*, 1800413; b) C. Crivello, S. Sevim, O. Graniel, C. Franco, S. Pané, J. Puigmartí-Luis, D. Muñoz-Rojas, *Mater. Horiz.* **2020**, *8*, 168–178.
[15] J. Liu, C. Wöll, *Chem. Soc. Rev.* **2017**, *46*, 5730–5770.
[16] H. A. Schulze, B. Hoppe, M. Schäfer, D. P. Warwas, P. Behrens, *ChemNanoMat* **2019**, *5*, 1159–1169.
[17] B. Hoppe, K. D. J. Hindricks, D. P. Warwas, H. A. Schulze, A. Mohmeyer, T. J. Pinkvos, S. Zailskas, M. R. Krey, C. Belke, S. König et al., *CrystEngComm* **2018**, *20*, 6458–6471.
[18] G. E. Gomez, F. Roncaroli, *Inorg. Chim. Acta* **2020**, *513*, 119926.
[19] J. Luo, Y. Li, H. Zhang, A. Wang, W.-S. Lo, Q. Dong, N. Wong, C. Povinelli, Y. Shao, S. Chereddy et al., *Angew. Chem. Int. Ed.* **2019**, *58*, 15313–15317.
[20] a) P. Horcajada, C. Serre, D. Grosso, C. Boissière, S. Perruchas, C. Sanchez, G. Férey, *Adv. Mater.* **2009**, *21*, 1931–1935; b) Z. Hu, C. Tao, H. Liu, X. Zou, H. Zhu, J. Wang, *J. Mater. Chem. A* **2014**, *2*, 14222.
[21] Y. Huang, C. Tao, R. Chen, L. Sheng, J. Wang, *Nanomaterials* **2018**, *8*, 676.
[22] E. Redel, Z. Wang, S. Walheim, J. Liu, H. Gliemann, C. Wöll, *Appl. Phys. Lett.* **2013**, *103*, 91903.
[23] a) O. Shekhah, *Materials* **2010**, 1302–1315; b) Z.-G. Gu, J. Zhang, *Coord. Chem. Rev.* **2019**, *378*, 513–532.
[24] E. Virmani, J. M. Rotter, A. Mähringer, T. von Zons, A. Godt, T. Bein, S. Wuttke, D. D. Medina, *J. Am. Chem. Soc.* **2018**, *140*, 4812–4819.
[25] J. Shankwitz, D. Speed, D. Sinanan, G. Szulczewski, *Inorganics* **2021**, *9*, 1.
[26] a) S. Han, R. A. Ciufo, M. L. Meyerson, B. K. Keitz, C. B. Mullins, *J. Mater. Chem. A* **2019**, *7*, 19396–19406; b) I. Stassen, M. Styles, G. Grenci, H. van Gorp, W. Vanderlinden, S. D. Feyter, P. Falcaro, D. D. Vos, P. Vereecken, R. Ameloot, *Nat. Mater.* **2016**, *15*, 304–310; c) T. Stassin, S. Rodríguez-Hermida, B. Schrode, A. J. Cruz, F. Carraro, D. Kravchenko, V. Creemers, I. Stassen, T. Hauffman, D. D. Vos et al., *Chem. Commun.* **2019**, *55*, 10056–10059; d) T. Stassin, I. Stassen, J. Marreiros, A. J. Cruz, R. Verbeke, M. Tu, H. Reinsch, M. Dickmann, W. Egger, I. F. J. Vankelecom et al., *Chem. Mater.* **2020**, *32*, 1784–1793.
[27] G. Lu, J. T. Hupp, *J. Am. Chem. Soc.* **2010**, *132*, 7832–7833.
[28] M. Miyamoto, S. Kohmura, H. Iwatsuka, Y. Oumi, S. Uemiya, *CrystEngComm* **2015**, *17*, 3422–3425.
[29] C.-H. Chuang, J.-H. Li, Y.-C. Chen, Y.-S. Wang, C.-W. Kung, *J. Phys. Chem. C* **2020**, *124*, 20854–20863.
[30] Z. Dou, J. Yu, H. Xu, Y. Cui, Y. Yang, G. Qian, *Thin Solid Films* **2013**, *544*, 296–300.
[31] a) O. Shekhah, H. Wang, S. Kowarik, F. Schreiber, M. Paulus, M. Tolan, C. Sternemann, F. Evers, D. Zacher, R. A. Fischer et al., *J. Am. Chem. Soc.* **2007**, *129*, 15118–15119; b) Z. Wang, K. Rodewald, R. Medishetty, B. Rieger, R. A. Fischer, *Cryst. Growth Des.* **2018**, *18*, 7451–7459.
[32] A. Demessence, C. Boissière, D. Grosso, P. Horcajada, C. Serre, G. Férey, G. J. A. A. Soler-Illia, C. Sanchez, *J. Mater. Chem.* **2010**, *20*, 7676–7681.
[33] C. Zhang, Y. Zhao, Y. Li, X. Zhang, L. Chi, G. Lu, *Chem. Asian J.* **2016**, *11*, 207–210.
[34] G. Wißmann, A. Schaate, S. Lilienthal, I. Bremer, A. M. Schneider, P. Behrens, *Microporous Mesoporous Mater.* **2012**, *152*, 64–70.
[35] H. Furukawa, F. Gándara, Y.-B. Zhang, J. Jiang, W. L. Queen, M. R. Hudson, O. M. Yaghi, *J. Am. Chem. Soc.* **2014**, *136*, 4369–4381.
[36] F. Fathieh, M. J. Kalmutzki, E. A. Kapustin, P. J. Waller, J. Yang, O. M. Yaghi, *Sci. Adv.* **2018**, *4*, eaat3198.
[37] J. Choi, L.-C. Lin, J. C. Grossman, *J. Phys. Chem. C* **2018**, *122*, 5545–5552.
[38] G. Zahn, H. A. Schulze, J. Lippke, S. König, U. Sazama, M. Fröba, P. Behrens, *Microporous Mesoporous Mater.* **2015**, *203*, 186–194.
[39] G. Zahn, P. Zerner, J. Lippke, F. L. Kempf, S. Lilienthal, C. A. Schröder, A. M. Schneider, P. Behrens, *CrystEngComm* **2014**, *16*, 9198–9207.
[40] a) C. G. Piscopo, A. Polyzoidis, M. Schwarzer, S. Loebbecke, *Microporous Mesoporous Mater.* **2015**, *208*, 30–35; b) M. R. DeStefano, T. Islamoglu, S. J. Garibay, J. T. Hupp, O. K. Farha, *Chem. Mater.* **2017**, *29*, 1357–1361; c) Z. Chen, X. Wang, H. Noh, G. Ayoub, G. W. Peterson, C. T. Buru, T. Islamoglu, O. K. Farha, *CrystEngComm* **2019**, *21*, 2409–2415.
[41] S. Zhou, O. Shekhah, A. Ramírez, P. Lyu, E. Abou-Hamad, J. Jia, J. Li, P. M. Bhatt, Z. Huang, H. Jiang et al., *Nature* **2022**, *606*, 706–712.
[42] S. Li, S. Zhang, D. Dai, T. Li, *Inorg. Chem.* **2021**, *60*, 11750–11755.
[43] J. Sun, Q. Li, G. Chen, J. Duan, G. Liu, W. Jin, *Sep. Purif. Technol.* **2019**, *217*, 229–239.
[44] K. Zhan, Y. Zhu, J. Yan, Y. Chen, *Phys. Lett. A* **2020**, *384*, 126678.
[45] W. Chen, Z. Zhang, L. Hou, C. Yang, H. Shen, K. Yang, Z. Wang, *Sep. Purif. Technol.* **2020**, *250*, 117198.
[46] H. Liu, B. Li, Y. Zhao, C. Kong, C. Zhou, Y. Lin, Z. Tian, L. Chen, *Chem. Commun.* **2021**, *57*, 13008–13011.
[47] P. Iacomi, F. Formalik, J. Marreiros, J. Shang, J. Rogacka, A. Mohmeyer, P. Behrens, R. Ameloot, B. Kuchta, P. L. Llewellyn, *Chem. Mater.* **2019**, *31*, 8413–8423.
[48] J. Zhang, H.-J. Bai, Q. Ren, H.-B. Luo, X.-M. Ren, Z.-F. Tian, S. Lu, *ACS Appl. Mater. Interfaces* **2018**, *10*, 28656–28663.
[49] a) H. Kim, S. Yang, S. R. Rao, S. Narayanan, E. A. Kapustin, H. Furukawa, A. S. Umans, O. M. Yaghi, E. N. Wang, *Science* **2017**, *356*, 430–434; b) M. J. Kalmutzki, C. S. Diercks, O. M. Yaghi, *Adv. Mater.* **2018**, *30*, 1704304.
[50] M. V. Solovyeva, L. G. Gordeeva, T. A. Krieger, Y. Aristov, *Energy Convers. Manag.* **2018**, *174*, 356–363.
[51] M. Thommes, K. Kaneko, A. V. Neimark, J. P. Olivier, F. Rodriguez-Reinoso, J. Rouquerol, K. S. Sing, *Pure Appl. Chem.* **2015**, *87*, 1051–1069.
[52] T. Druffel, O. Buazza, M. Lattis, S. Farmer, M. Spencer, N. Mandzy, E. A. Grulke, *Nanophotonic Materials V* **2008**, *7030*, 70300F.
[53] N. C. Keppler, K. D. J. Hindricks, P. Behrens, *RSC Adv.* **2022**, *12*, 5807–5815.
[54] B. Han, A. Chakraborty, *Appl. Therm. Eng.* **2020**, *175*, 115393.
[55] T. Stassin, R. Verbeke, A. J. Cruz, S. Rodríguez-Hermida, I. Stassen, J. Marreiros, M. Krishtab, M. Dickmann, W. Egger, I. F. J. Vankelecom et al., *Adv. Mater.* **2021**, *33*, 2006993.
[56] D. Zhang, Y. Zhu, L. Liu, X. Ying, C.-E. Hsiung, R. Sougrat, K. Li, Y. Han, *Science* **2018**, *359*, 675–679.
[57] C. Altintas, O. F. Altundal, S. Keskin, R. Yildirim, *J. Chem. Inf. Model.* **2021**, *61*, 2131–2146.

Manuscript received: August 10, 2023
Revised manuscript received: September 12, 2023
Accepted manuscript online: September 15, 2023
Version of record online: September 27, 2023